



Experimental study on hydrodynamic characteristics of the box-type floating breakwater with different mooring configurations

Jia-ming Liang, Yong Liu*, Yong-kun Chen, Ai-jun Li

Shandong Provincial Key Laboratory of Ocean Engineering, Ocean University of China, Qingdao, 266100, China

ARTICLE INFO

Keywords:
 Box-type floating breakwater
 Mooring system
 Experimental test
 Hydrodynamic characteristic
 Motion response
 Mooring force

ABSTRACT

The box-type floating breakwater is simple and durable, which is one important type of floating breakwaters. In this paper, a systematic experimental study on the hydrodynamic characteristics of the box-type floating breakwater is performed in a wave flume, and the influence of the mooring system on the wave attenuation performance of the box-type floating breakwater is studied. The transmission coefficients, reflection coefficients, energy dissipation coefficients, motion responses and mooring forces of the box floating breakwater under the fixed condition and three different mooring configurations are compared and analyzed. The experimental results show that the box-type floating breakwater under the fixed condition has better wave attenuation performance than that under the mooring condition. The cross mooring and parallel mooring configurations without section lying on the seabed are more effective in reflecting and dissipating longer period waves. The results also indicate that there is obvious difference in motion responses of the breakwater under different mooring configurations, and the mooring forces are affected by the motion responses. A reasonable choice of mooring configurations is more conducive to ensuring the safety of floating breakwaters and improving the wave attenuation performance.

1. Introduction

Compared with bottom-mounted breakwater, floating breakwater consisting of a floating body and a mooring system has the advantages of lower engineering cost, rapid construction, easy demolition, and no effect from seabed topography condition. Floating breakwaters are often used for the protection of marina, marine ranches and offshore structures. In addition, some operation area at sea usually requires relatively calm sea condition, and temporary floating breakwaters are often used to protect the operation area.

Many scholars have been committed to improving the performance of the floating breakwater and studying its wave dissipation mechanism. [Dai et al. \(2018\)](#) categorized floating breakwaters into seven structural types, including pontoon type, horizontal plate type, frame type and so on. [Sutko \(1975\)](#) studied the hydrodynamic performance of floating breakwaters with rectangular, triangular, and circular cross-sections, and the results showed that the box-type floating breakwater with a rectangular cross-section had better wave attenuation performance. The box-type floating breakwater has a simple geometric cross-section and can operate stably in the ocean, so it is an important type of floating breakwaters. [Black et al. \(1971\)](#) studied the hydrodynamic

characteristics of a fixed rectangular floating breakwater. A breakwater in a fixed condition does not generate radiation waves, so the hydrodynamic characteristics of a fixed floating breakwater are simpler than those of floating breakwater in a floating condition. [Drimer et al. \(1992\)](#) developed an analytical solution to the two-dimensional hydrodynamic problem of wave interaction with a box-type floating breakwater, and they indicated that the box-type floating breakwater had good wave attenuation performance in the case of moderate depth water. [Zheng et al. \(2004\)](#) used the matched eigenfunction expansion method to obtain analytical expressions for the velocity potentials of radiation and diffraction waves due to a rectangular floating breakwater. Based on the research of [Zheng et al. \(2004\)](#), [Zheng and Zhang \(2015\)](#) solved the wave diffraction and radiation problems of multiple rectangular floating bodies, and explored the influence of structural parameters on the hydrodynamic quantities. [Masoudi and Gan \(2020\)](#) developed a theoretical model to predict the performance of a submerged floating rectangular breakwater, and the theoretical results were in good agreement with the results of the boundary element method. For numerical research, [Rahman et al. \(2006\)](#) and [Saghi et al. \(2021\)](#) used the Volume Of Fluid (VOF) method, [Peng et al. \(2013\)](#) combined the direct-forcing Immersed Boundary (IB) method and the VOF method to study the hydrodynamic

* Corresponding author.

E-mail address: liuyong@ouc.edu.cn (Y. Liu).

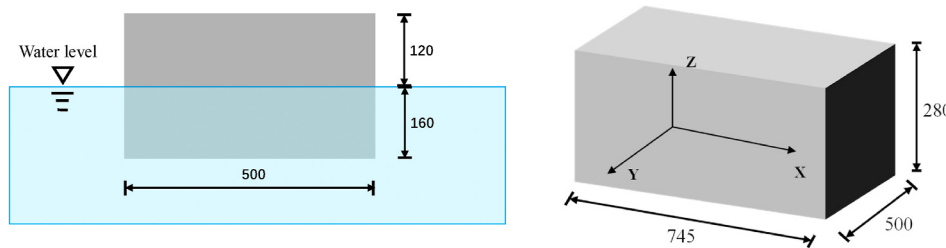


Fig. 1. Details of the physical model sketch (Unit: mm).

performance of the inclined-moored rectangular floating breakwater. Ren et al. (2017), Liu et al. (2019) and Liu and Wang (2020) adopted Smoothed Particles Hydrodynamics (SPH) model to study nonlinear wave interaction with the rectangular floating body. Based on the Reynolds Average Navier-Stokes (RANS) equation, Islam et al. (2019) studied the hydrodynamic performance of the box-type floating breakwater through the OpenFOAM, an open-source computational fluid dynamics framework.

The wave dissipation mechanism around floating breakwaters is complicated. In addition to numerical and analytical methods, experimental research is an effective method to solve such complicated problems. Koutandos et al. (2010) investigated the hydrodynamic performance of the rectangular floating breakwater with fixed and heave motion conditions under the action of regular waves and irregular waves through an experimental test. The results showed that the reflection coefficient of the heave motion breakwater was less than that of the fixed breakwater. Loukogeorgaki et al. (2014) conducted a three-dimensional experimental study on the hydrodynamic characteristics of multiple longitudinally flexibly connected box-type floating breakwaters under the action of oblique waves. The performance of a box-floating breakwater in different terrains was investigated by Cui et al. (2019) in a physical model test. Ji et al. (2018) experimentally studied the hydrodynamic characteristics of double-row rectangular floating breakwaters, and indicated that the double-row floating breakwater had better wave attenuation ability than the single-row floating breakwater. In recent years, the integrated systems of box-type breakwaters and wave energy converters (WEC) have also attracted the attention of many scholars (He et al., 2013; Ning et al., 2016; Zhao and Ning, 2018; Zhao et al., 2019; Jalani et al., 2022). They indicated that the integrated breakwater-WEC systems improved the wave attenuation performance of breakwaters and could convert wave energy into electric energy.

The mooring system is an important part of the floating breakwater, and its layout and structural parameters will influence the hydrodynamic performance of the floating breakwater. Yamamoto et al. (1980)

developed a two-dimensional numerical model to study the performance of the floating breakwater under different mooring configurations. They found that under the cross mooring configuration, if a reasonable stiffness coefficient was selected, the wave attenuation ability for longer waves could be significantly improved. Sannasiraj et al. (1998) adopted two-dimensional finite element method and experimental tests to study the hydrodynamic performance of the rectangular floating breakwater under three different mooring methods. The results showed that the mooring forces were greatly influenced by the mooring configuration, and the transmission coefficient under the cross mooring configuration was larger than that under the other two mooring configurations. Elchahal et al. (2009) developed a numerical model to study the influence of the mooring chain stiffness, mooring angle and other parameters on the performance of the box-type floating breakwater. Yoon et al. (2018) compared the hydrodynamic performance of the perforated-type rectangular floating breakwaters under catenary and tension-leg systems. Their results showed that the tension-leg system led to larger mooring force and smaller transmission coefficient. Dong et al. (2008) revealed that a floating breakwater with a shorter length of the chain lying (LCL) on the sea bottom had better wave attenuation performance. The reason was that the small LCL restricted the movement of the breakwater and blocked more wave energy.

By summarizing previous studies, it can be found that most of the research on the different mooring system for floating breakwater focused on the theoretical and numerical research, and there were few systematic experimental investigations. In comparison to numerical and theoretical methods, experiments may be closer to reality and more reliable. It is necessary to carry out experimental research on the hydrodynamic characteristics of floating breakwaters under different mooring systems. Choosing an appropriate mooring system is helpful to improve the wave attenuation performance of the floating breakwater. On the other hand, increasing the width and draft of the box-type floating breakwater (a simple and durable floating breakwater) can effectively improve the wave attenuation ability (Wang et al., 2010; He et al., 2012), but it will also increase the engineering cost. In order to better design floating breakwaters, it is necessary to well study its hydrodynamic characteristics. In this paper, a systematic experimental study on the hydrodynamic characteristics of the fixed and the moored box-type floating breakwater is carried out in a wave flume. The transmission coefficients, reflection coefficients, energy dissipation coefficients, motion responses and mooring forces are comprehensively investigated. The hydrodynamic characteristics of the box-type floating breakwater under three different mooring configurations are discussed, and the hydrodynamic characteristics of the box-type floating breakwater under the fixed condition and the box-type floating breakwater under different mooring configurations are compared. This paper aims to provide a comprehensive understanding for the hydrodynamic characteristics of the box-type floating breakwater. The characteristics of different mooring systems are revealed, hoping to provide a reference for the design of mooring systems in practice engineering.

2. Experimental tests

This experiment was carried out in a wave flume at the Shandong



Fig. 2. Physical model used in the experiment.

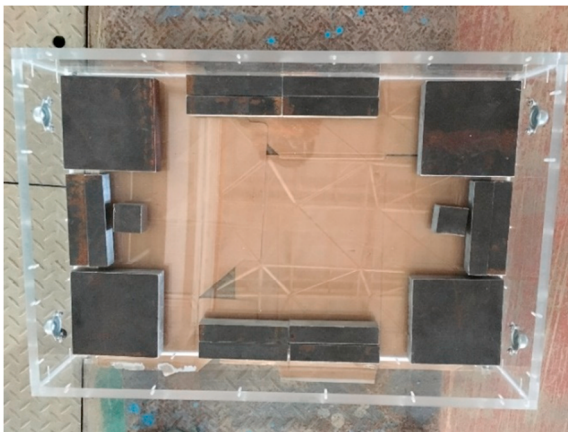


Fig. 3. Special steel ballast.



Fig. 4. Device for measuring the center of gravity and the moment of inertia.

Provincial Key Laboratory of Ocean Engineering, Ocean University of China. The glass-walled wave flume was equipped with a piston-type wave maker at one end and a porous energy-dissipating slope at the other end to absorb waves, so that the wave flume could stably create target waves. The flume was 3 m wide, 60 m long, and 1.8 m deep. The scale of this experiment was 1:20. The flume was divided into two channels of 0.8 m and 2.2 m by glass plates, and the experiment was carried out in the 0.8 m wide channel.

2.1. Floating breakwater model

The width B of the rectangular floating breakwater used in the experiment was 0.5 m, the length L_m was 0.745 m, the height H_m was 0.28 m and the model draft D was 0.16 m. The schematic diagram of the model is shown in Fig. 1. The model was made of 15 mm thick acrylic plates, as shown in Fig. 2. The model draft was adjusted to 0.16 m through customized steel ballast (as shown in Fig. 3). The ballasts were fixed at the bottom of the model to prevent the ballast from moving during the experiment and affecting the measurement accuracy.

The gravity center and the inertia moment of the model were measured by a special device that can rotate around the axis. The device is shown in Fig. 4. The model after the counterweight was placed on the



Fig. 5. The ball bearing.

device to measure the oscillation period T around the horizontal axis, and the radius of gyration was calculated by the following formula:

$$T = 2\pi \sqrt{\frac{W_1 l_1^2 + W_2 [(z_o - z_{G1})^2 + K_{yy}^2]}{g[W_1(z_o - z_{G1}) + W_2(z_o - z_{G2})]}} \quad (1)$$

$$l_1 = \sqrt{\left(\frac{T_1}{2\pi}\right)^2 g(z_o - z_{G1})} \quad (2)$$

where W_1 is the weight of the section frame (rotatable part), W_2 is the weight of the measured model, l_1 is the radius of gyration for the section frame around the axis of rotation, z_o , z_{G1} , z_{G2} , respectively, are the distance from the upper surface of the section frame to the axis of rotation, the vertical position of the center of gravity for the section frame, and the vertical position of the center of gravity for the measured model, K_{yy} is the radius of gyration for the measured model, g is the acceleration of gravity, T_1 is the oscillation period of the section frame, and T is the oscillation period of the measured model.

The inertia moment of the model was measured at least three times, and the average value was taken as the inertia moment of the model. The detailed model parameters are listed in Table 1.

The ball bearings were assembled on both sides of the model to restrict the model to a two-dimensional motion track, as shown in Fig. 5. The small ball can rotate in different directions to prevent collision and friction between the model and the flume sidewall during the experiment to ensure measurement accuracy.

2.2. Mooring system

The box-type floating breakwater model was moored at a distance of 30 m from the wave maker using a catenary mooring system. Each mooring line was made of stainless steel with a line density of 0.177 kg/m. A spring was used to simulate the stiffness of the mooring chain with a stiffness coefficient of 2.36 kN/m. The spring was a specially customized spring with a diameter similar to that of the mooring chain to prevent nonlinear factors from affecting the experimental results.

The cross mooring system is a commonly used mooring method in practice (Peña et al., 2011). In this study, it is applied to floating breakwaters to explore its wave attenuation performance. Three

Table 1

Detailed parameters of the physical models.

Model	Length (mm)	Bottom breadth (mm)	Height (mm)	Draught (mm)	Mass (kg)	Moment of inertia ($\text{kg}\cdot\text{m}^2$)	Gravity Center above bottom (mm)
Floating breakwater	745	500	280	160	58.09	2.441	65.2

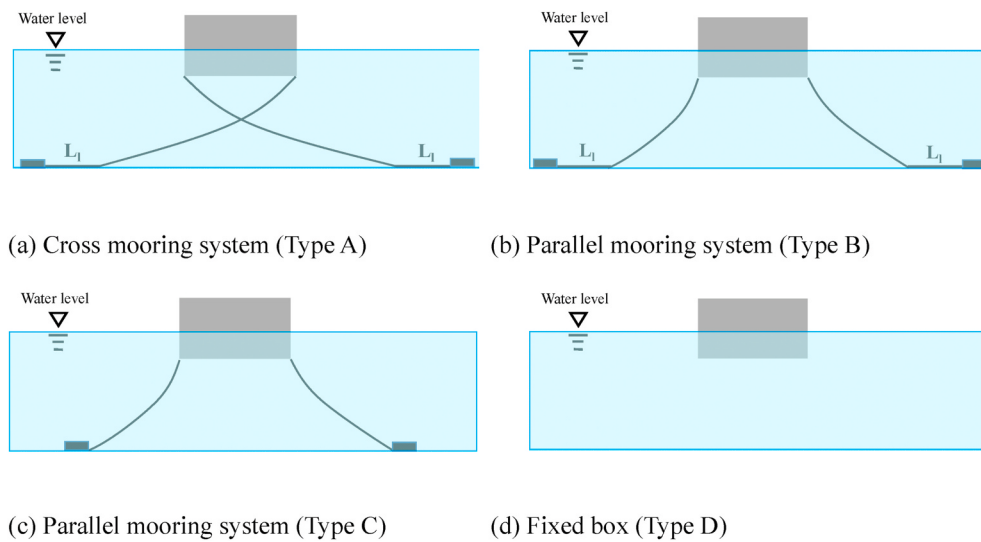


Fig. 6. Four different mooring configurations.

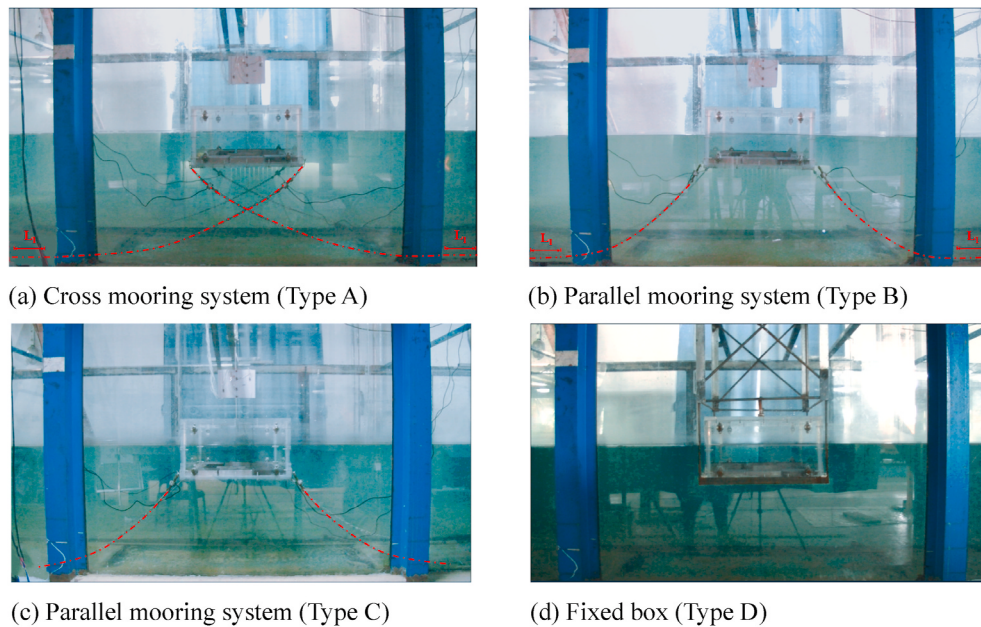


Fig. 7. Four different mooring configurations used in the experiment. (: The position of the mooring chain.)

Table 2
Detailed parameters of the mooring system.

Mooring system	Chain length (cm)	Lying the floor length L_f (cm)	Stiffness coefficient (kN/m)
Cross mooring system (Type A)	156.7	32.6	2.36
Parallel mooring system (Type B)	112.5	32.6	2.36
Parallel mooring system (Type C)	80.9	0	2.36
Fixed box (Type D)	/	/	/

mooring configurations were used in the experiment: (1) Cross mooring system (Type A), (2) Parallel mooring system with section lying on the seabed (Type B), (3) Parallel mooring system without section lying on the seabed (Type C), (4) The box-type floating breakwater in a fixed condition (Type D). The schematic diagrams of different mooring

configurations are shown in Fig. 6. The mooring chain materials and stiffness coefficients of all mooring configurations were the same. The anchor point was arranged at the bottom of the flume according to the requirements of the mooring configuration, and the mooring chain was connected to the anchor point. The experimental layout is shown in Fig. 7. The position of the mooring chain is marked with a red dotted line for readers to view. The specific mooring chain parameters are shown in Table 2. The box-type floating breakwater in the fixed condition was suspended in the water by a special steel frame, and the draft was the same as that of the floating breakwater in the mooring condition.

2.3. Data collection and analysis

The experimental setup is shown in Fig. 8. The water depth was fixed at 0.6 m in all the tests. A broad range of wave conditions was adopted to ensure that the hydrodynamic characteristics of the box-type floating breakwater could be comprehensively understood. The wave period ranged from 1 s to 1.8 s, and the wave height ranged from 0.05 m to 0.15

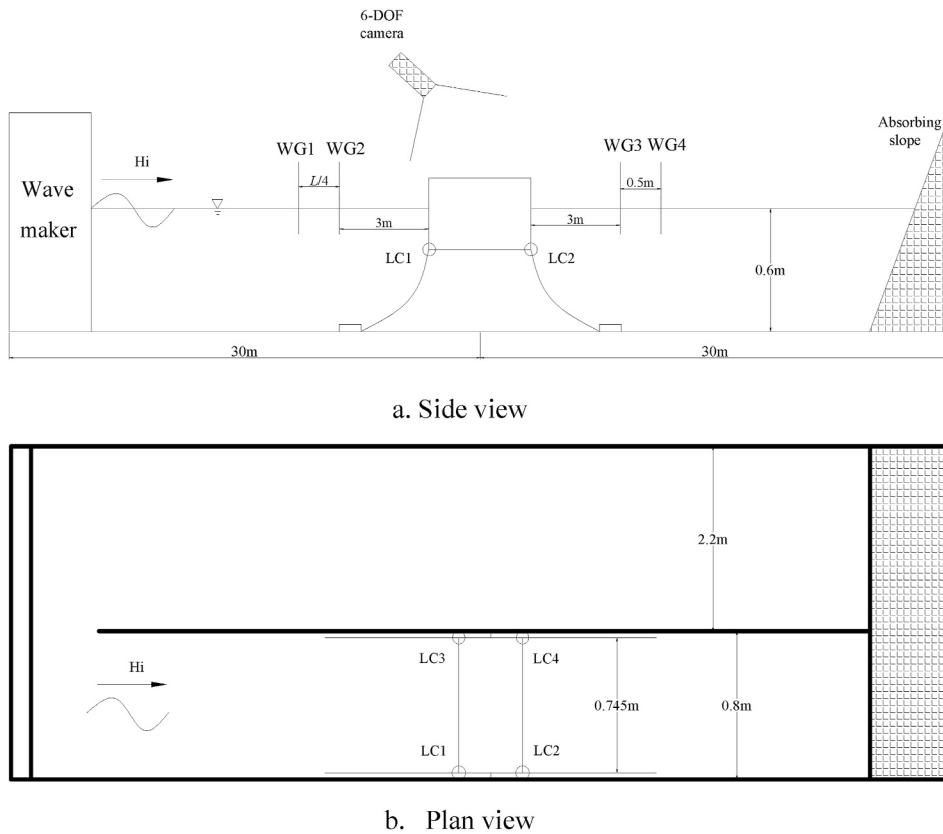


Fig. 8. Sketch of the experimental setup for the box-type breakwater.

Table 3

The wave parameters and water depth used in the tests.

Wave height H (m)	Wave period T (s)	Water depth h (m)
0.05	1.2	0.6
0.07	1, 1.1, 1.2, 1.4, 1.6, 1.8	
0.10	1, 1.1, 1.2, 1.4, 1.6, 1.8	
0.13	1, 1.1, 1.2, 1.4, 1.6, 1.8	
0.15	1.2	

m. According to the research of Cui et al. (2019), the ratio of the breakwater width to the wavelength B/L (L is the wavelength) was an important parameter that affected the performance of breakwater. The range of B/L in this experiment was 0.131–0.325. The detailed wave conditions are listed in Table 3.

Four wave gauges with a sampling frequency of 50 Hz were used to measure the wave surface elevation. Two wave gauges (WG1 and WG2) were placed in front of the floating breakwater to record the resultant surface elevation of incident and reflected waves. Then, the incident wave height H_i and the reflected wave height H_r were separated through the two-point method proposed by Goda and Suzuki (1976). The distance between the wave gauges WG1 and WG2 was $L/4$ (L is the wavelength) as recommended by Dean and Dalrymple (1984). Two wave gauges (WG3 and WG4) were placed on the leeward side of the floating breakwater to record the surface elevation of the transmitted waves, and the average value was taken as the transmitted wave height H_t . The transmission coefficient (K_t), the reflection coefficient (K_r) and the energy dissipation coefficient (K_d) are defined as

$$K_t = \frac{H_t}{H_i} \quad (3)$$

$$K_r = \frac{H_r}{H_i} \quad (4)$$

$$K_d = 1 - K_r^2 - K_t^2 \quad (5)$$

Four circular load cells and a 64-channel CRONOS PL16-DCB8 data acquisition instrument were used to record mooring forces. Considering that the load cell placed at the bottom end of the mooring chain may cause friction with the ground to affect the experimental results, four load cells were respectively connected to the upper part of the mooring chain. The measured windward mooring force is F_w , and the leeward mooring force is F_l . The dimensionless mooring forces (C_{Fw} , C_{Fl}) are defined as

$$C_{Fw} = \frac{F_w}{\rho g H B} \quad (6)$$

$$C_{Fl} = \frac{F_l}{\rho g H B} \quad (7)$$

The motion responses of the floating breakwater were recorded by the Optotrak Certus System (E-type), which was composed of system control unit, data collection software, host computer, etc. Since the motion response was limited to a two-dimensional range, the motion responses of three degrees of freedom (surge, heave and roll) were obtained by placing markers on the breakwater model. Dimensionless parameters of response amplitude operators (RAOs) are used to discuss the motion response of the box-type floating breakwater. The response amplitude operators of surge, roll and heave are defined as

$$R_s = \frac{A_{\text{surge}}}{A_i} \quad (8)$$

$$R_r = \frac{A_{\text{roll}}}{A_i} \quad (9)$$

$$R_h = \frac{A_{\text{heave}}}{A_i} \quad (10)$$

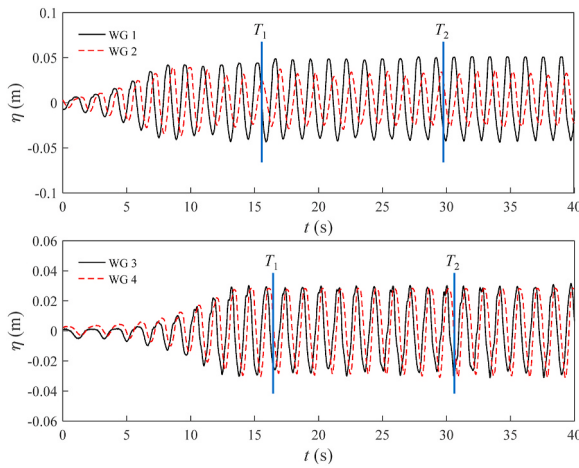


Fig. 9. Time histories of surface elevations η measured by WG 1, 2, 3 and 4 probes for Type A floating breakwater at: $H = 0.07$ m and $T = 1.4$ s.

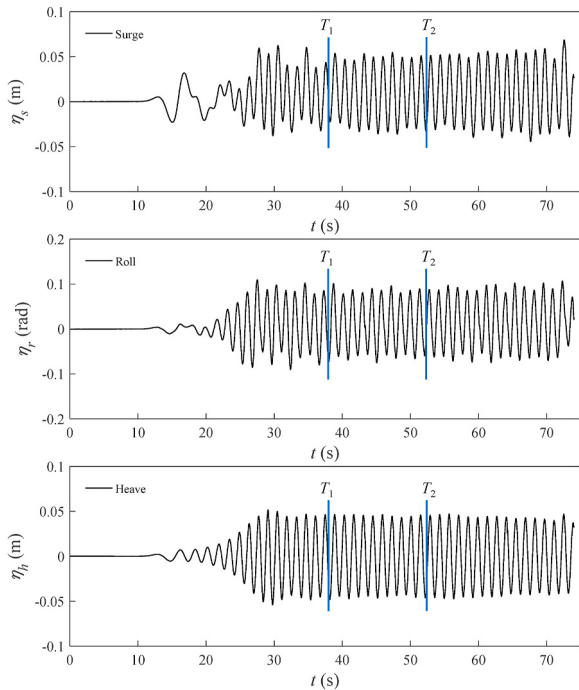


Fig. 10. Time histories of surge, roll and heave (η_s , η_r , η_h) for Type A floating breakwater at: $H = 0.07$ m and $T = 1.4$ s.

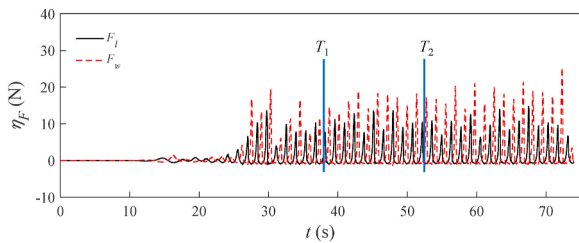


Fig. 11. Time histories of mooring force η_F for Type A floating breakwater at: $H = 0.07$ m and $T = 1.4$ s.

All measuring instruments were calibrated before the experiment to ensure the accuracy of the collected data. Figs. 9–11 show the typical time histories of free surface elevation, motion response and mooring

forces, respectively. The experimental results H_b , H_r , H_b , A_{surge} , A_{roll} , A_{heave} , F_w and F_l were obtained based on the stable elevations (between T_1 and T_2). More time history results of the measured mooring forces are given in the Appendix.

3. Transmission, reflection and energy dissipation coefficients

3.1. Comparison between experimental and BEM results

The boundary element method (BEM) has been used to solve the transmission coefficient and reflection coefficient of the box-type floating breakwater in a fixed condition. In this numerical method, the hydrodynamic problem for wave interaction with the fixed breakwater was solved by considering the following boundary integral equation:

$$\frac{1}{2}\varphi(\xi, \eta) = \int_{\Gamma} \left[\varphi(x, z; \xi, \eta) \frac{\partial G(x, z; \xi, \eta)}{\partial n} - G(x, z; \xi, \eta) \frac{\partial \varphi(x, z)}{\partial n} \right] d\Gamma(x, z) \quad (11)$$

$$G(x, z; \xi, \eta) = \frac{1}{2\pi} \ln \sqrt{(x - \xi)^2 + (z - \eta)^2} \quad (12)$$

where φ is the velocity potential of the fluid motion, Γ denotes the boundary curve of fluid domain, (x, z) and (ξ, η) are the field point and source point, respectively, $\partial/\partial n$ is the unit outward normal vector, $G(x, z; \xi, \eta)$ is the fundamental solution of Laplace equation.

The boundary curve Γ is discretized into a series of elements, and a system of linear equations are obtained from Eq. (11). Incorporating appropriate boundary conditions, the velocity potential and its normal derivation are solved on each boundary element. Thus, various hydrodynamic quantities can be obtained. The detailed solution process can be found in the previous study (Liu et al., 2012).

The comparison between the experimental results and the BEM results is shown in Fig. 12, where k represents the wave number. It can be seen that the experimental results, especially the transmission coefficient, are in good agreement with the BEM results. As for the reflection coefficient, Fig. 12 shows that the BEM results are slightly greater than the experimental results. Slight overestimation is mainly due to the fact that the BEM solution based on the potential theory cannot consider the energy dissipation caused by the flow separation near the box corners.

3.2. Transmission coefficient

Fig. 13 shows the variation of the transmission coefficient versus the dimensionless parameter H/L at $T = 1.2$ s for the box-type floating breakwater under different mooring configurations. As shown in Fig. 13, the transmission coefficients of Type A, Type B and Type C floating breakwaters increase with the increase of H/L . This indicates that the blocking effect of the floating breakwater on waves becomes worse as the wave height increases. In addition, the motion of the floating breakwater increases with the increase of wave height, which may generate larger radiation waves and make the transmitted waves larger. Larger motion-radiated waves are often considered to be unfavorable for wave attenuation (Ruol et al., 2013). For Type D floating breakwater, the transmission coefficient slightly decreases with the increase of H/L . This phenomenon is probably linked to the growing intensity in wave interaction with the fixed breakwater with the increasing wave height, which increases the dissipation of wave energy. As shown in Fig. 21, the energy dissipation coefficient of Type D floating breakwater increases with the increase of H/L .

As shown in Fig. 13, the wave attenuation performance of Type D floating breakwater is better than that of Type A, Type B and Type C floating breakwaters when $H/L > 0.033$. For instance, the transmission coefficient of the Type D floating breakwater is 34.3% smaller than that of Type B floating breakwater at $H/L = 0.071$.

When $H = 0.07$, 0.10 and 0.13 m, the variation of the transmission

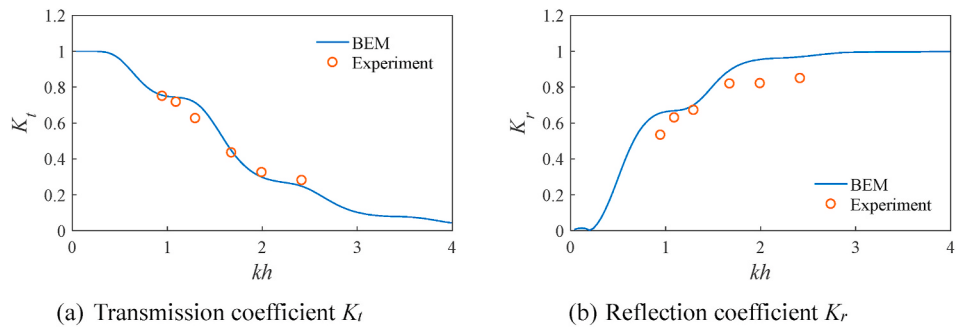


Fig. 12. Comparison between the experimental data and the BEM results at: $H = 0.07$ m and $h = 0.6$ m.

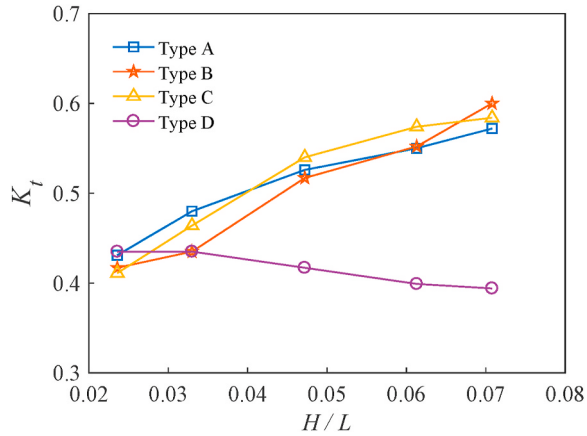


Fig. 13. Variation of the transmission coefficient K_t versus H/L ($T = 1.2$ s).

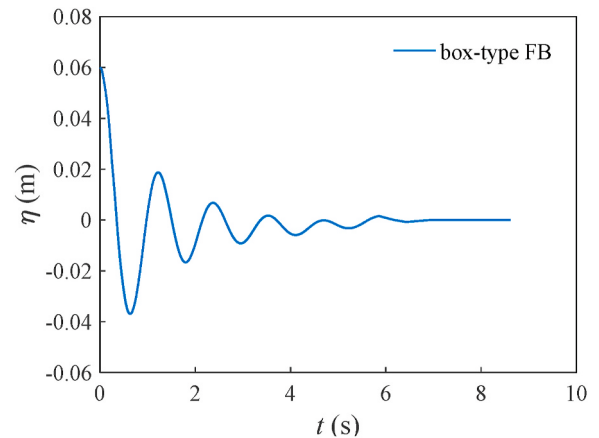


Fig. 15. The time series of the decay test for the box-type floating breakwater.

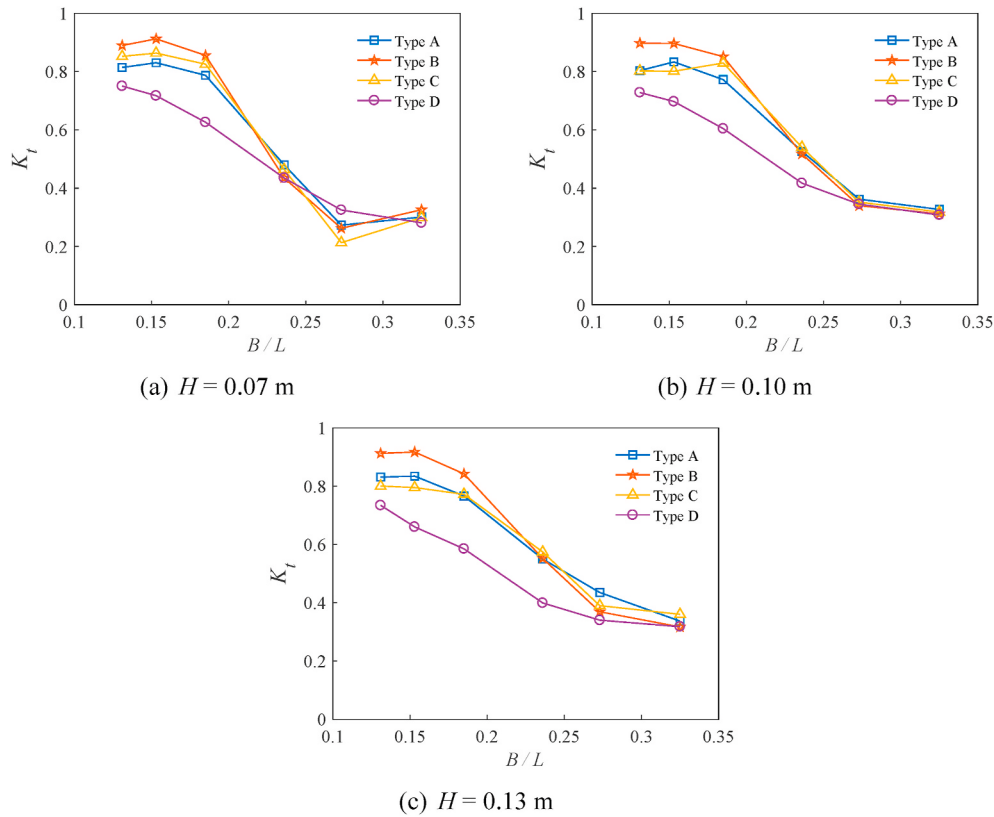


Fig. 14. Variation of the transmission coefficient K_t versus B/L at different incident wave height H .

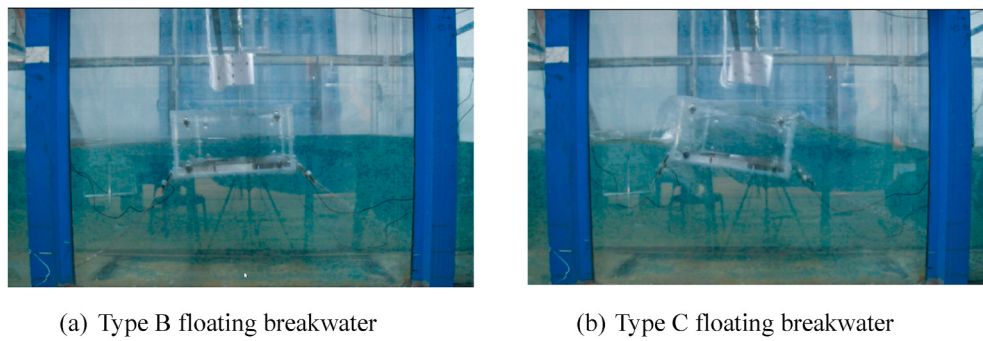


Fig. 16. Comparison of the interactions between wave and floating breakwater at: $T = 1.8$ s and $H = 0.13$ m.

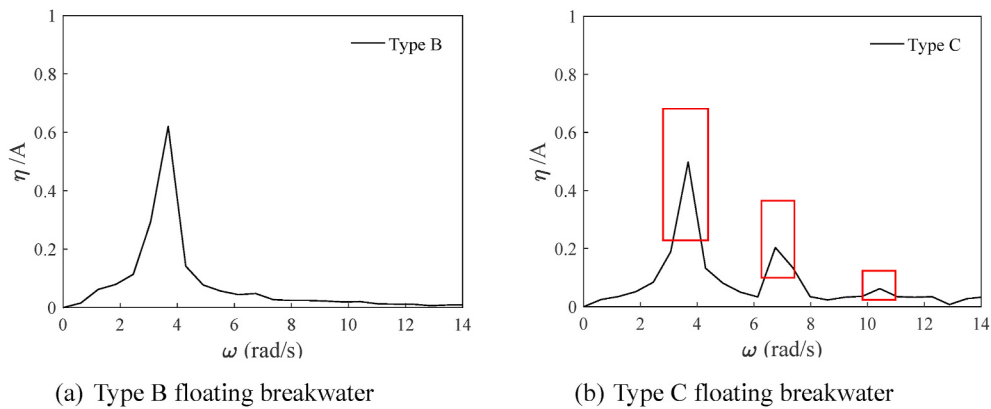


Fig. 17. Amplitude spectrums of the wave elevations on the leeside of the floating breakwater at: $T = 1.8$ s and $H = 0.13$ m.

coefficient versus the dimensionless parameter B/L for the box-type floating breakwater under different mooring configurations is shown in Fig. 14. It can be observed that the transmission coefficients of the box-type floating breakwaters all decrease with the increase of B/L . The transmission coefficient of Type D floating breakwater is mostly smaller than that of Type A, Type B and Type C floating breakwaters, which indicates the wave attenuation performance is better. When $H = 0.07$ m and $B/L = 0.273$, a special phenomenon of sudden decrease occurs in the transmission coefficients of Type A, Type B and Type C floating breakwaters, resulting in a minimum value. The main reason is that the transmission coefficient is affected by the natural period of the box-type floating breakwater. We measured the natural period of Type A, Type B and Type C floating breakwaters to be 1.1 s, and the corresponding value of B/L was 0.273. The time series of the decay test for the model is shown

in Fig. 15. When the wave height is small, the transmission coefficient of the model decreases due to the influence of the natural period. With the increase of wave height, the motion of the model increases and the interaction between waves and the model becomes more noticeable. The influence of the natural period on the transmission coefficient is rapidly weakened, and thus this phenomenon disappears in the case of $H = 0.10$ and 0.13 m.

It can be seen that Type A, Type B and Type C floating breakwaters have good wave attenuation performance for shorter waves and the variations of transmission coefficients are relatively similar. For longer waves, the transmission coefficient of Type A floating breakwater is smaller than that of Type B floating breakwater. Through the analysis of the motion response in the following Fig. 24, it can be known that for longer waves, the roll motion of Type A floating breakwater increases. Roll motion is considered to be beneficial to improve the wave attenuation performance of the breakwater (Huang et al., 2014). Larger roll motion increases the relative velocity between the corners of the breakwater and the surrounding water, which enhances the vortex shedding and dissipates more wave energy. For longer waves, the transmission coefficient of Type C floating breakwater is smaller than that of Type B floating breakwater, and with the increase of wave height, the transmission coefficient of Type C floating breakwater continues to decrease and is gradually smaller than that of Type A floating breakwater. The reason can be explained as follows. The box-type floating breakwater with long mooring chain will move in phase with the waves for longer waves and the wave attenuation performance is poor. The mooring chain of Type C breakwater (with short mooring chain) will be sudden straightened for longer waves, which leads to relatively rigid behavior of the floating breakwater against the incident wave, as shown in Fig. 16. FFT method is used for spectrum analysis of the wave surface on the leeward side of the box-type floating breakwater. Only fundamental frequency wave is separated from the leeward side of Type B floating breakwater, while double frequency and triple frequency waves

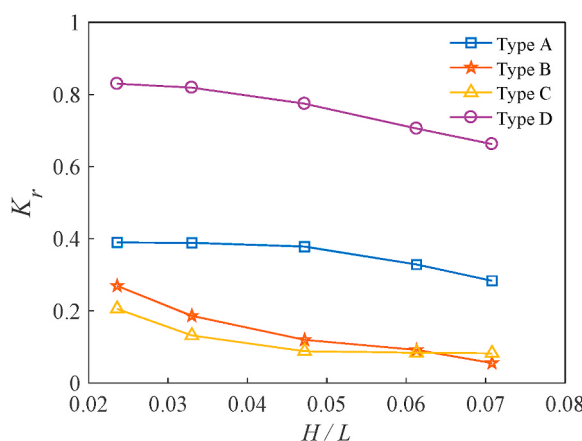


Fig. 18. Variation of the reflection coefficient K_r versus H/L ($T = 1.2$ s).

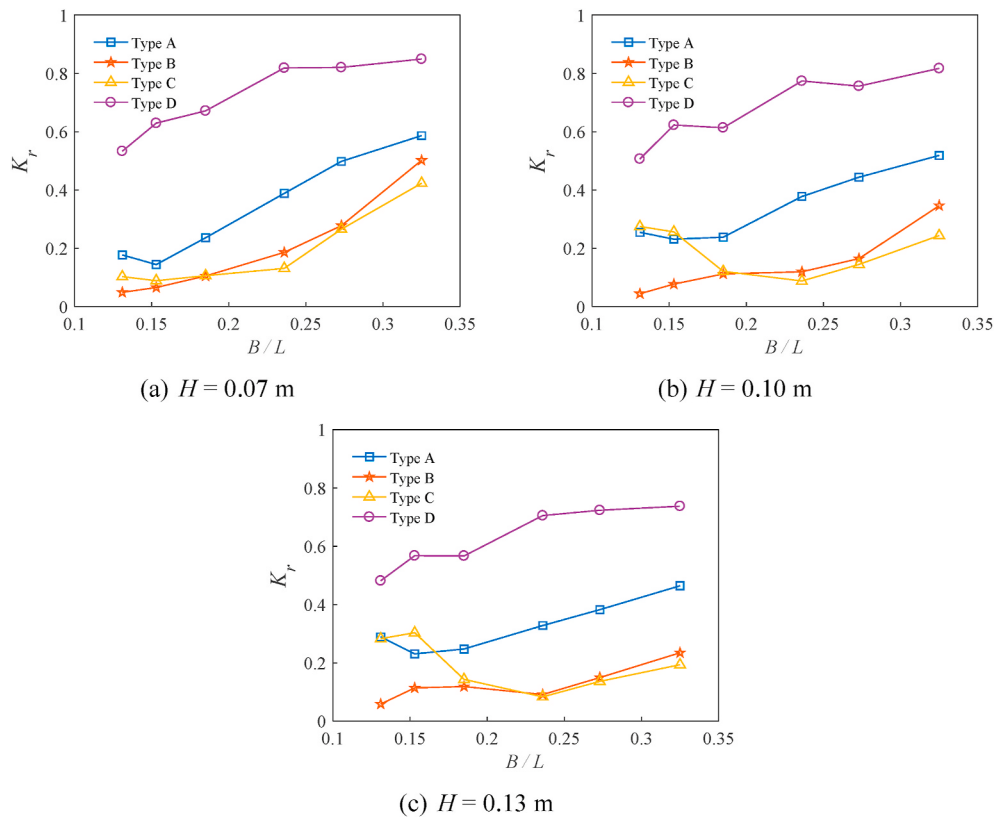


Fig. 19. Variation of the reflection coefficient K_r versus B/L at different incident wave height H .

appear on the leeward side of Type C floating breakwater. The amplitude spectrums of the wave elevations on the leeside of the floating breakwater are shown in Fig. 17. In the figure, η/A is the dimensionless wave amplitude, ω is the angular frequency. Due to the effect of mooring chain with a smaller length, the interaction between water waves and Type C breakwater should be more intense, which leads to radiation waves with high frequency. Thus, higher-order wave components are generated in transmitted waves. The violent interactions cause the Type C floating breakwater to dissipate more wave energy. Therefore, with the increase of wave height, the box-type floating breakwater under parallel mooring configuration without section lying on the seabed (Type C) has better attenuation performance for longer waves.

3.3. Reflection coefficient

The reflection coefficient is an important parameter of the floating breakwater. Fig. 18 shows the variation of the reflection coefficient versus the dimensionless parameter H/L at $T = 1.2 \text{ s}$ for the box-type floating breakwater under different mooring configurations. It can be

seen from the figure that the reflection coefficient of the box-type floating breakwater all decreases slightly with the increase of H/L . The reflection coefficients of Type A, Type B and Type C floating breakwaters are less than that of Type D floating breakwater. Among them, the average reflection coefficient of Type C floating breakwater is 84.7% smaller than that of Type D floating breakwater at $H/L = 0.024\text{--}0.071$.

For the box-type floating breakwater in the mooring condition, the floating breakwater under the cross mooring configuration (Type A) has a larger reflection coefficient. The average reflection coefficient of the floating breakwater under the cross mooring configuration is 230% greater than that of Type C floating breakwater at $H/L = 0.024\text{--}0.071$. It can be observed that the reflection coefficient of Type C floating breakwater is slightly smaller than that of Type B floating breakwater at $H/L < 0.062$, but the opposite result appears at $H/L > 0.062$.

When $H = 0.07, 0.10$ and 0.13 m , the variation of the reflection coefficient versus the dimensionless parameter B/L for the box-type floating breakwater under different mooring configurations is shown in Fig. 19. In the whole B/L range, the reflection coefficient of Type D

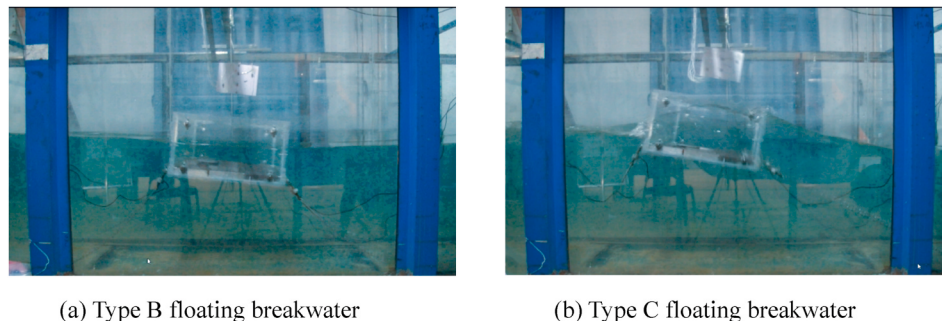


Fig. 20. Snapshots of the interaction between waves and the breakwater at: $T = 1.6 \text{ s}$ and $H = 0.13 \text{ m}$.

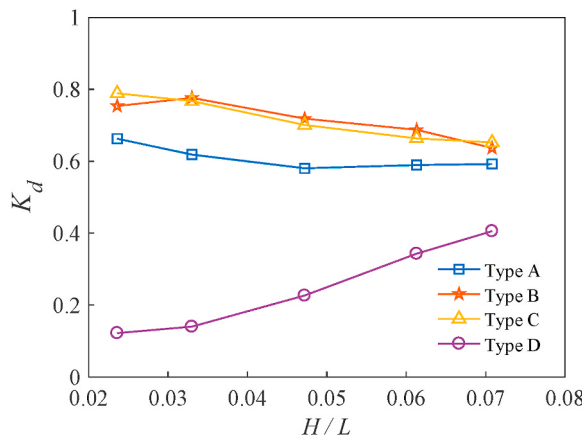


Fig. 21. Variation of the energy dissipation coefficient K_d versus H/L ($T = 1.2$ s).

floating breakwater is greater than that of Type A, Type B and Type C floating breakwaters.

The reflection coefficient of the floating breakwater under the cross mooring configuration is greater than that of the other two parallel mooring configurations except for some longer wave conditions. For shorter waves, the reflection coefficient of Type C floating breakwater is slightly smaller than that of Type B floating breakwater. For longer waves, the reflection coefficient of Type C floating breakwater is greater than that of Type B floating breakwater, and this trend becomes more obvious with the increase of wave height. The increase in reflection coefficient is probably linked to the fact that the floating breakwater with the shorter mooring chain will be straightened for longer waves. Then, the floating breakwater will block more waves and increase the reflection coefficient, as shown in Fig. 20.

3.4. Energy dissipation coefficient

Fig. 21 shows the variation of the energy dissipation coefficient versus the dimensionless parameter H/L at $T = 1.2$ s for the box-type floating breakwater under different mooring configurations. It can be seen from the figure that the energy dissipation coefficients of Type A, Type B and Type C floating breakwaters slightly decrease with the increase of H/L . For Type D floating breakwater, the energy dissipation coefficient increases with the increase of H/L . The energy dissipation coefficient of the fixed floating breakwater is smaller than that of the floating breakwater under other mooring configurations. There is little difference in the energy dissipation coefficient between the Type B and Type C floating breakwaters, and the average energy dissipation coefficient of Type A floating breakwater is 14.6% smaller than that of Type B floating breakwater at $H/L = 0.024\text{--}0.071$.

When $H = 0.07, 0.10$ and 0.13 m, the variation of the energy dissipation coefficient versus the dimensionless parameter B/L for the box-type floating breakwater under different mooring configurations is shown in Fig. 22. It reveals that the energy dissipation coefficients of Type A, Type B and Type C floating breakwaters increase with the increase of B/L , indicating the wave energy dissipation under longer wave conditions is smaller than that under shorter wave conditions. The wave energy dissipation coefficient of the fixed floating breakwater changes little with B/L , and most of them are smaller than that of Type A, Type B and Type C floating breakwaters, especially when $H = 0.07$ m. The energy dissipation coefficient of Type A floating breakwater is smaller than that of type B floating breakwater for shorter waves, and the opposite conclusion appears for longer waves. The energy dissipation coefficient of Type C floating breakwater is similar to that of Type B floating breakwater for shorter waves, but is larger than that of Type B floating breakwater for longer waves. With the increase of wave height, the energy dissipation coefficient of Type C floating breakwater is gradually larger than that of Type A floating breakwater for longer waves. Combined with the reflection coefficient, it can be concluded that the energy dissipation is the main way to attenuate the wave for the

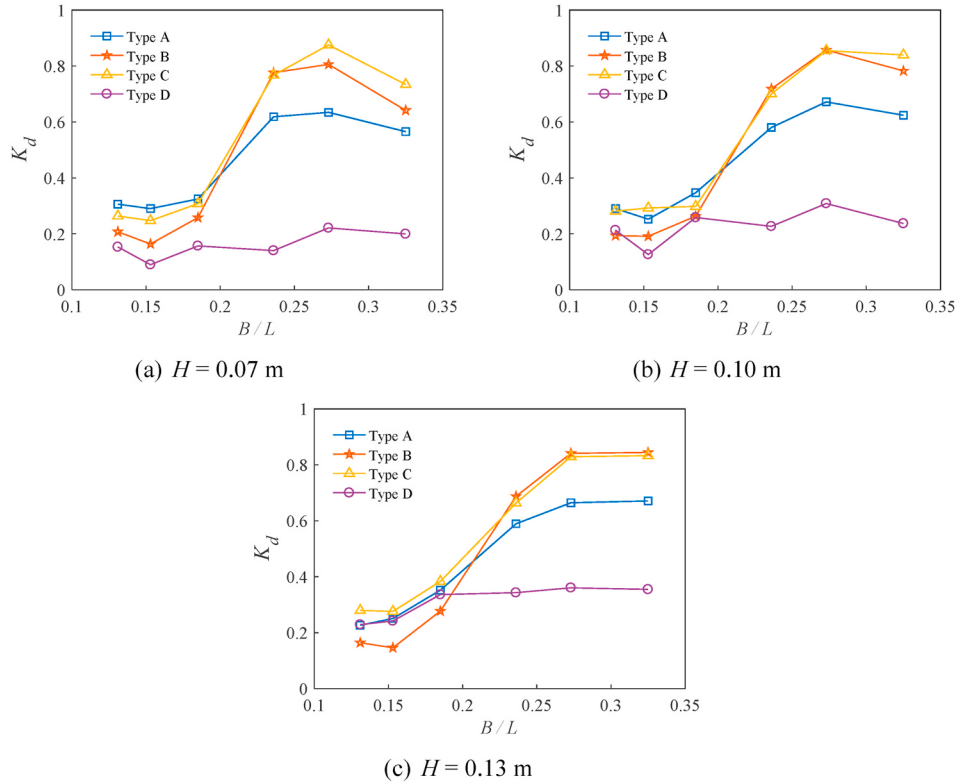


Fig. 22. Variation of the energy dissipation coefficient K_d versus B/L at different incident wave height H .

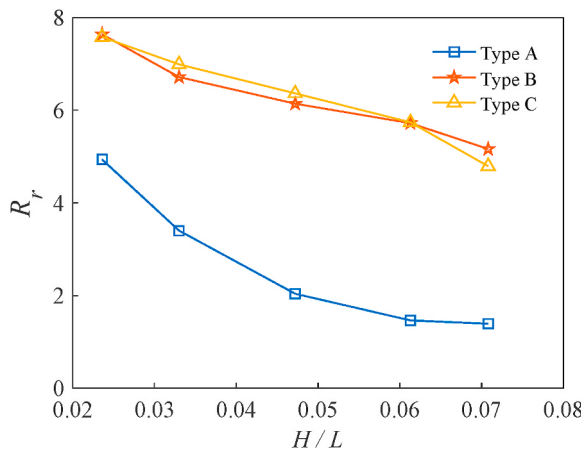


Fig. 23. Variation of the roll motion R_r versus H/L ($T = 1.2$ s).

box-type floating breakwater in the mooring condition. But, the wave reflection is the main way to reduce transmitted wave height for the box-type floating breakwater in the fixed condition.

4. Motion response

In order to better understand the wave dissipation mechanism of the box-type floating breakwater, the motion response characteristics of the breakwater are discussed in this section.

4.1. Roll motion

Fig. 23 shows the variation of the roll RAO versus the dimensionless parameter H/L at $T = 1.2$ s for the box-type floating breakwater under different mooring configurations. It can be seen that the roll RAO of

Type A, Type B and Type C floating breakwaters decreases with the increase of H/L . In the entire H/L range, there is no significant difference in roll RAOs between Type B floating breakwater and Type C floating breakwater, but they are larger than that of Type A floating breakwater. Among them, the average roll RAO of Type A floating breakwater is 60% smaller than that of Type C floating breakwater at $H/L = 0.024\text{--}0.071$.

When $H = 0.07, 0.10$ and 0.13 m, the variation of the roll RAO versus the dimensionless parameter B/L for the box-type floating breakwater under different mooring configurations is shown in Fig. 24. It is obvious that the roll RAO of Type B and Type C floating breakwaters increases with the increase of B/L when $B/L < 0.236$. While $B/L > 0.236$, the opposite trend appears, reaching the maximum at $B/L = 0.236$. The roll RAO of Type C floating breakwater increases when $B/L < 0.154$, which is greater than that of Type B floating breakwater.

It can be seen from the figure that the roll RAO of the floating

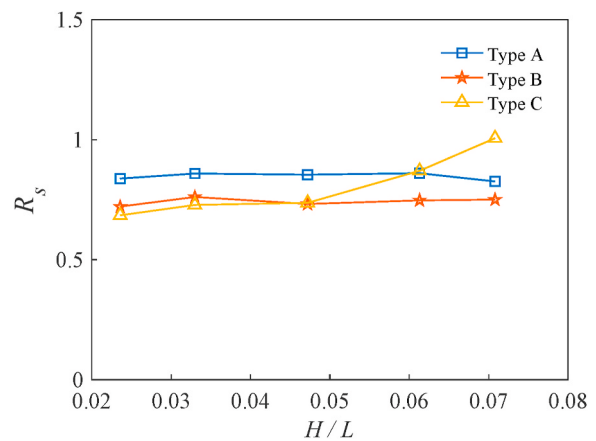


Fig. 25. Variation of the surge motion R_s versus H/L ($T = 1.2$ s).

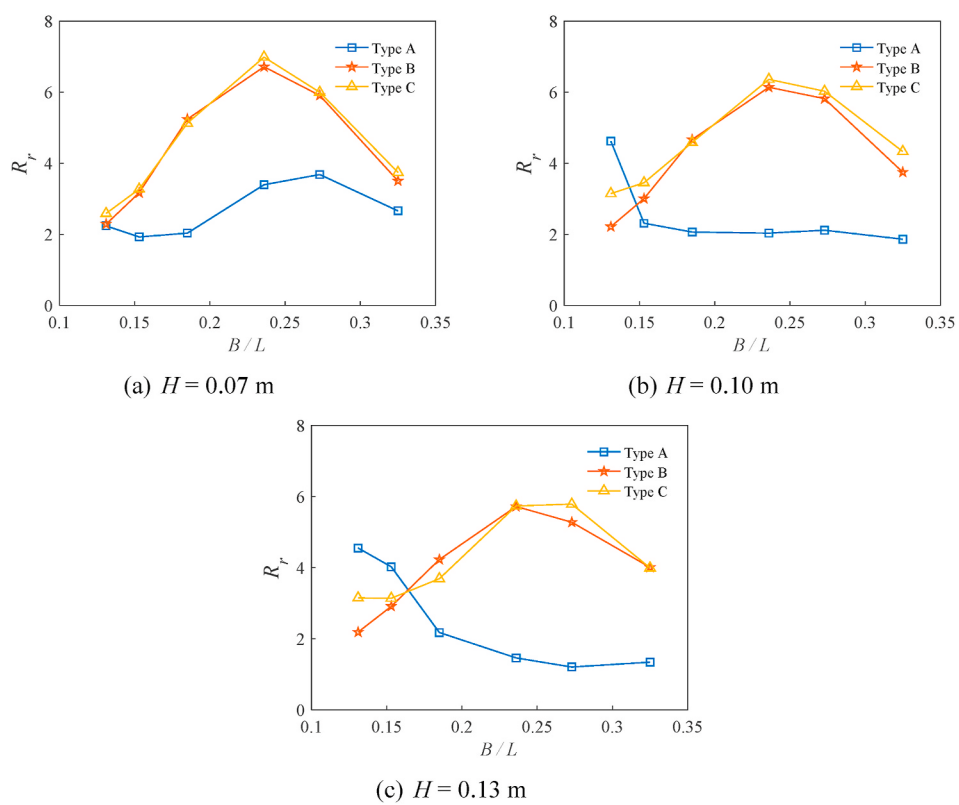


Fig. 24. Variation of the roll motion R_r versus B/L at different incident wave height H .

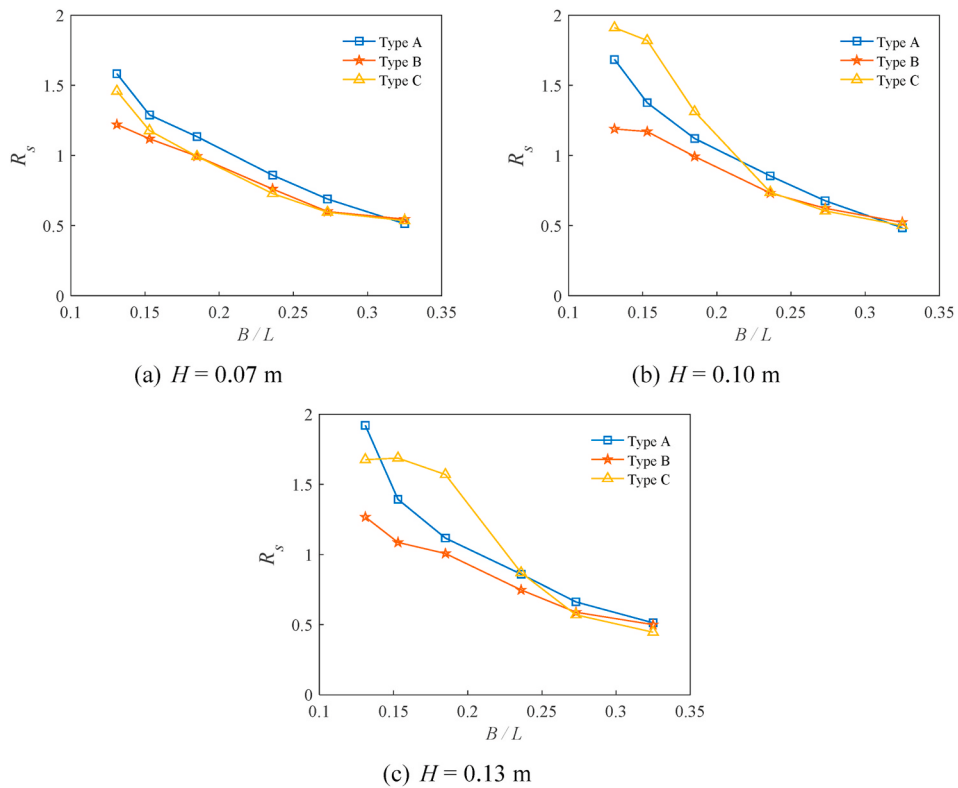


Fig. 26. Variation of the surge motion R_s versus B/L at different incident wave height H .

breakwater under the cross mooring configuration (Type A) is smaller than that under other two parallel mooring configurations. But as the wave height increases, the roll RAO of the floating breakwater under the cross mooring configuration increases in some longer wave conditions.

4.2. Surge motion

Fig. 25 shows the variation of the surge RAO versus the dimensionless parameter H/L at $T = 1.2 \text{ s}$ for the box-type floating breakwater under different mooring configurations. It can be seen from the figure that the surge RAO of Type A and Type B floating breakwaters keeps stable with the increase of H/L . The average surge RAO of Type A floating breakwater is 14.2% larger than that of Type B floating breakwater at $H/L = 0.024\text{--}0.071$. When $H/L < 0.047$, the surge RAO of Type C floating breakwater is smaller than that of Type A and Type B floating breakwaters. As the wave height increases, the surge RAO of Type C floating breakwater increases and is gradually larger than that of Type A and Type B floating breakwaters.

When $H = 0.07, 0.10$ and 0.13 m , the variation of the surge RAO versus the dimensionless parameter B/L for the box-type floating breakwater under different mooring configurations is shown in Fig. 26. It could be seen that the surge RAO of Type A, Type B and Type C floating breakwaters all decreases with the increase of B/L . When $H = 0.07, 0.10$ and 0.13 m , the surge RAO of Type A floating breakwater is larger than Type B floating breakwater except for $B/L = 0.325$. The surge RAO of Type C floating breakwater is closer to Type B floating breakwater for shorter waves. But for longer waves, the surge RAO of Type C floating breakwater increases rapidly as the wave height increases. The main reason for this phenomenon is that the mooring chain is short, causing the breakwater to oscillate back and forth under longer wave conditions, which increases the surge motion. With reference to Figs. 25 and 26, it can conclude that the surge motion of the floating breakwater under parallel mooring configuration without section lying on the seabed is more sensitive to the wave height.

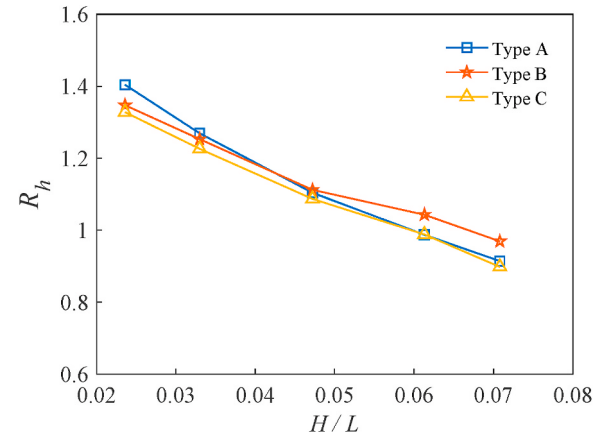


Fig. 27. Variation of the heave motion R_h versus H/L ($T = 1.2 \text{ s}$).

4.3. Heave motion

Fig. 27 shows the variation of the heave RAO versus the dimensionless parameter H/L at $T = 1.2 \text{ s}$ for the box-type floating breakwater under different mooring configurations. It can be seen that the heave RAOs of Type A, Type B and Type C floating breakwaters are similar, and all decrease with the increase of H/L .

When $H = 0.07, 0.10$ and 0.13 m , the variation of the heave RAO versus the dimensionless parameter B/L for the box-type floating breakwater under different mooring configurations is shown in Fig. 28. The heave RAO of Type A, Type B and Type C floating breakwaters decreases with the increase of B/L . The heave RAO of Type A and Type B floating breakwaters has little difference. The heave RAO of Type C floating breakwater is smaller than that of Type A and Type B floating breakwaters when $B/L < 0.236$, especially at $H = 0.10 \text{ m}$ and 0.13 m . As the wave height increases, the heave RAO of Type C floating breakwater

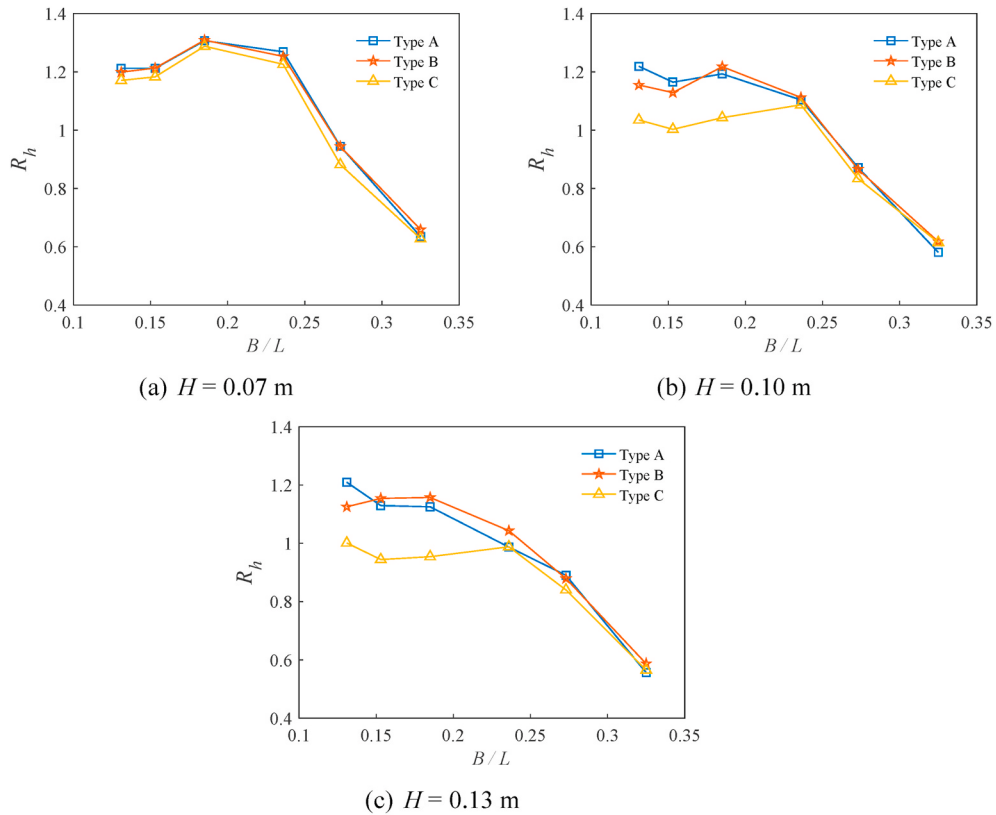


Fig. 28. Variation of the heave motion R_h versus B/L at different incident wave height H .

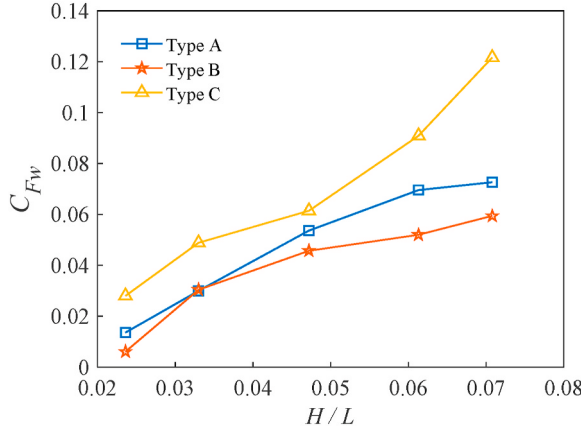


Fig. 29. Variation of the windward mooring force C_{Fw} versus H/L ($T = 1.2$ s).

slightly decreases for longer waves. The main reason is that the short mooring chain imposes greater restraining forces on the breakwater, resulting in less heave motion.

5. Mooring force

The mooring system is an important part of the floating breakwater. The mooring forces are affected by the wave condition and the motion responses of the breakwater, so understanding its mechanism can ensure safe and stable work of the breakwater.

Figs. 29 and 30 show the variation of the mooring forces versus the dimensionless parameter H/L at $T = 1.2$ s for the box-type floating breakwater under different mooring configurations. It can be seen from the figure that both C_{Fw} and C_{Fl} increases with the increase of H/L , and C_{Fw} is larger than C_{Fl} . When $T = 1.2$ s, C_{Fw} of Type C floating breakwater

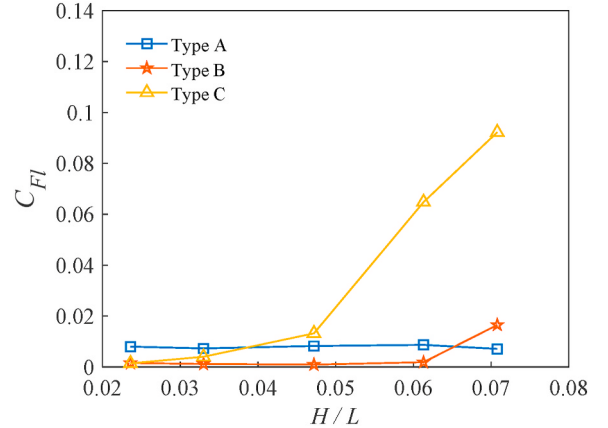


Fig. 30. Variation of the leeward mooring forces C_{Fl} versus H/L ($T = 1.2$ s).

increases rapidly with the increase of H/L , which is greater than that of Type A and Type B floating breakwaters. Among them, the average C_{Fw} of Type B floating breakwater is 47.1% smaller than that of Type C floating breakwater at $H/L = 0.024\text{--}0.071$. The floating breakwater under parallel mooring system with section lying on the seabed has smaller mooring forces. C_{Fl} of Type A, Type B and Type C floating breakwaters is relatively small and has little change when $H/L < 0.047$. But when $H/L > 0.047$, C_{Fl} of Type C floating breakwater increases sharply. It can be concluded that the mooring forces of Type C floating breakwater are more sensitive to the wave height. The main reason is that as the wave height increases, the interaction between the floating breakwater with a short mooring chain and the waves becomes stronger. Thus, the mooring forces of Type C floating breakwater increases sharply.

When $H = 0.07, 0.10$ and 0.13 m, the variation of C_{Fw} versus the

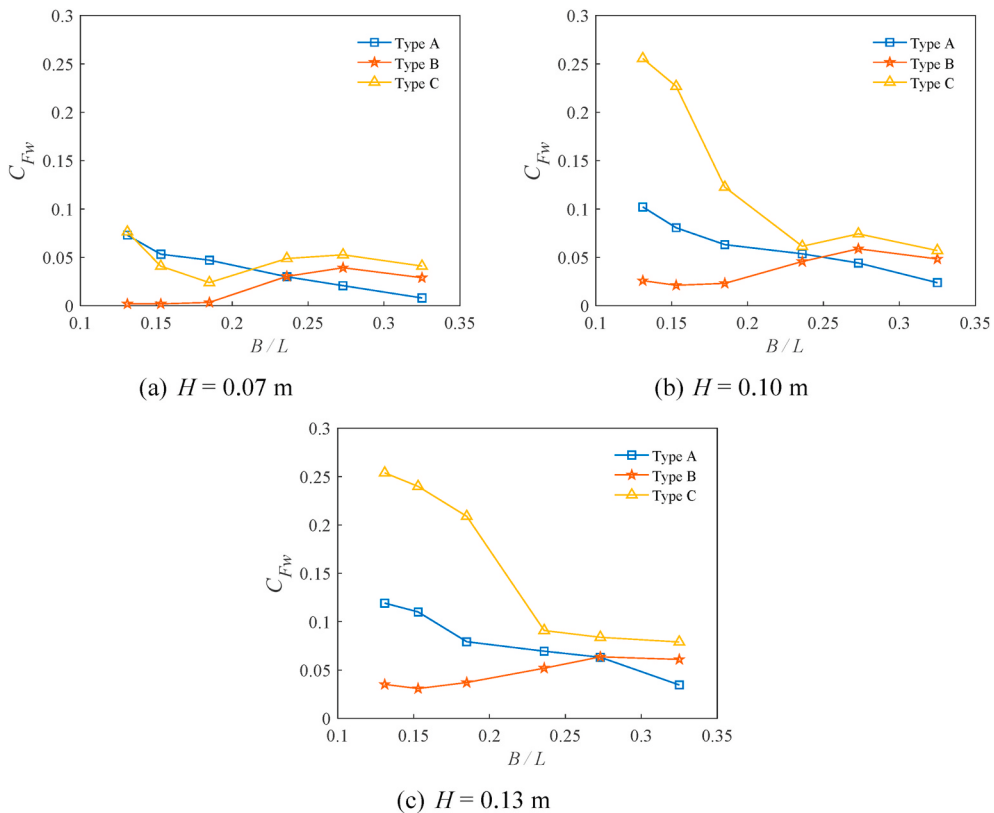


Fig. 31. Variation of the windward mooring forces C_{Fw} versus B/L at different incident wave height H .

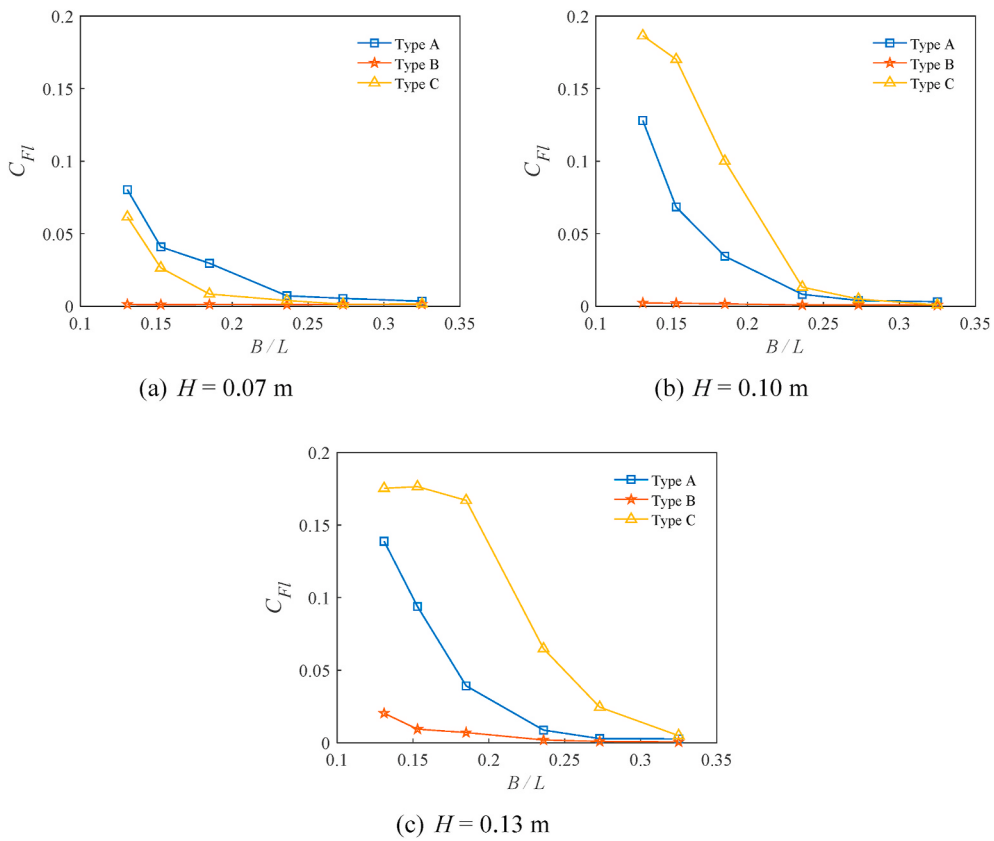


Fig. 32. Variation of the leeward mooring forces C_{Fl} versus B/L at different incident wave height H .

dimensionless parameter B/L under the different mooring configurations is shown in Fig. 31. It could be found that C_{Fw} of Type B floating breakwater increases with the increase of B/L when $B/L < 0.273$. While $B/L > 0.273$, the opposite trend appears, reaching the maximum at $B/L = 0.273$. When $B/L = 0.273$, the breakwater may be affected by the natural period, resulting in a large mooring force. For longer waves, the mooring forces gradually decrease. The reason may be that Type B floating breakwater move with waves for longer waves, causing an in-phase motion with the waves. The interaction between the breakwater and the waves is weakened, which reduce the mooring forces.

When $H = 0.07, 0.10$ and 0.13 m, C_{Fw} of Type A floating breakwater decreases with the increase of B/L . When $B/L < 0.236$, C_{Fw} of Type A floating breakwater is larger than that of Type B floating breakwater. However, there is a completely opposite trend when $B/L > 0.236$. The floating breakwater under the cross mooring configuration has a small motion response for shorter waves and has a larger motion response for longer waves. The mooring force is affected by the motion of the floating breakwater, resulting in this result.

When $H = 0.07$ m, C_{Fw} of Type C floating breakwater is greater than that of Type B floating breakwater in the entire B/L range. As the wave height increases, C_{Fw} of Type C floating breakwater increases rapidly, which is greater than that of the other two mooring configurations. According to the analysis in the previous chapters, as the wave height increases, the surge motion of Type C floating breakwater increases rapidly, resulting in a rapid increase in the mooring force. On the whole, C_{Fw} of the floating breakwater under parallel mooring configuration without section lying on the seabed is greater than that of the other two mooring configurations.

When $H = 0.07, 0.10$ and 0.13 m, the variation of C_{Fl} versus the dimensionless parameter B/L under the different mooring configurations is shown in Fig. 32. According to Fig. 32, C_{Fl} of Type A, Type B and Type C floating breakwaters all decreases with the increase of B/L . Compared with Fig. 31, we can see that C_{Fl} is smaller than C_{Fw} in the entire B/L range, especially for shorter waves, but as the wave period increases, the difference decreases. The reason is that the box-type floating breakwater under the shorter wave conditions is mainly driven by drifting force (Cui et al., 2019), and thus C_{Fw} is greater than C_{Fl} . As the wave period increases, the wave can provide sufficient time for the floating breakwater to respond to the wave. The box-type floating breakwater moves in phase with the waves, and the influence of the drifting force on the mooring forces gradually decreases, so the mooring forces on the leeward side are close to the mooring forces on the windward side.

In the entire B/L range, C_{Fl} of Type B floating breakwater is smaller than that of Type A and Type C floating breakwaters. When $H = 0.07$ m, C_{Fl} of Type A floating breakwater is greater than that of Type C floating breakwater. With the increase of the wave height, C_{Fl} of Type C floating breakwater increases sharply, which is greater than that of Type A floating breakwater.

6. Conclusions

In this paper, the hydrodynamic characteristics of the box-type floating breakwater were comprehensively studied through physical model tests under a broad range of wave conditions. Combined with the characteristics of motion responses and mooring forces, the wave attenuation performance of the box-type floating breakwater under three different mooring configurations was analyzed in detail. The hydrodynamic characteristics of the box-type floating breakwater under a fixed condition and the box-type floating breakwater under three different mooring configurations were compared. The following conclusions are drawn.

- (1) For the box-type floating breakwater in the mooring condition, the wave height attenuation is mainly due to the wave energy

dissipation by the box. For the fixed box-type floating breakwater, it mainly relies on reflecting waves to reduce transmitted wave height.

- (2) Compared with the box-type breakwaters in the mooring conditions, the fixed floating breakwater has the lowest transmission coefficient and the largest reflection coefficient. For longer waves, the wave attenuating performance of the box-type floating breakwaters under cross mooring configuration and parallel mooring configuration without section lying on the seabed is better. Yamamoto et al. (1980) also came to the same conclusion in their research, but Sannasiraj et al. (1998) showed that the transmission coefficient in the case of cross mooring configuration was greater than that of other mooring configurations. The reflection coefficient of the box-type floating breakwater under the cross mooring configuration is larger than that under the parallel mooring configurations. When the wave height is small, the transmission coefficient of the box-type floating breakwater in the mooring condition will be significantly reduced near the natural period. Sannasiraj et al. (1998) found that the transmission coefficient was not sensitive to mooring configurations. But, the present study have shown that the mooring configuration has a greater impact on the transmission coefficient for longer waves.
- (3) Floating breakwaters under different mooring configurations show different motion response characteristics. The roll motion of the box-type floating breakwater under the cross mooring configuration is smaller than that of the box-type floating breakwater under the parallel mooring configuration. The heave motion of the box-type floating breakwater under the parallel mooring configuration without section lying on the seabed is relatively smaller than that under other mooring configurations, especially for longer waves.
- (4) The mooring configuration has a significant impact on the mooring forces, which is similar to the conclusion of Sannasiraj et al. (1998). Among the three mooring configurations, the mooring forces of the box-type floating breakwaters under the parallel mooring configuration without section lying on the seabed are relatively large, and its mooring forces increase rapidly with the increase of wave height. The mooring forces of the box-type floating breakwaters under the parallel mooring configuration with section lying on the seabed are relatively small. The mooring forces near the natural period of the floating breakwater are greater. The mooring forces on the windward side is greater than the mooring forces on the leeward side.

CRediT authorship contribution statement

Jia-ming Liang: Methodology, Experimental tests, Formal analysis, Writing – original draft. **Yong Liu:** Conceptualization, Methodology, Formal analysis, Funding acquisition, Writing – review & editing. **Yong-kun Chen:** Experimental tests, Formal analysis, Writing – review & editing. . **Ai-jun Li:** BEM codes, Validation, Writing – review & editing.

Declaration of competing interest

The authors declare that they have no known competing financial interests or personal relationships that could have appeared to influence the work reported in this paper.

Acknowledgements

This study was supported by the National Natural Science Foundation of China (Nos. 51725903 and 52088102) and the Taishan Scholar Program of Shandong Province (No. ts20190915).

Appendix

Figs. A1 and A2 show the typical time histories of mooring forces in the experiment. The experimental test conditions are: (1) Type B floating breakwater, $H = 0.07$ m, $T = 1.4$ s and $d = 0.6$ m; (2) Type C floating breakwater, $H = 0.10$ m, $T = 1.4$ s and $d = 0.6$ m.

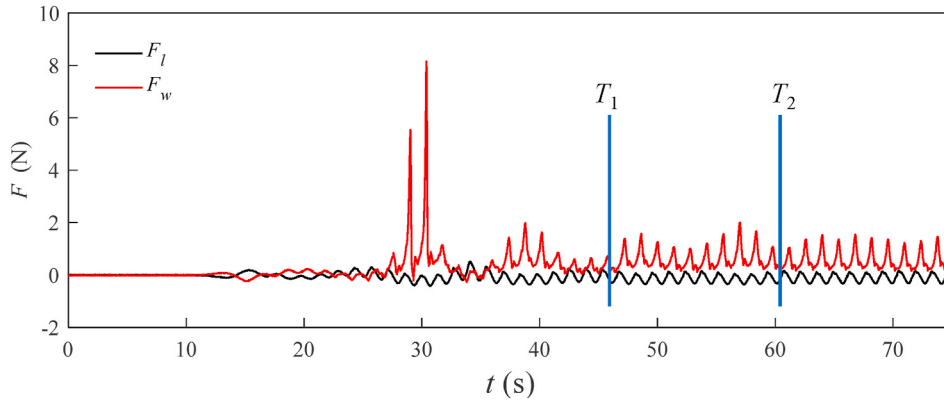


Fig. A1. Time histories of mooring force η_F for Type B floating breakwater at: $H = 0.07$ m and $T = 1.4$ s.

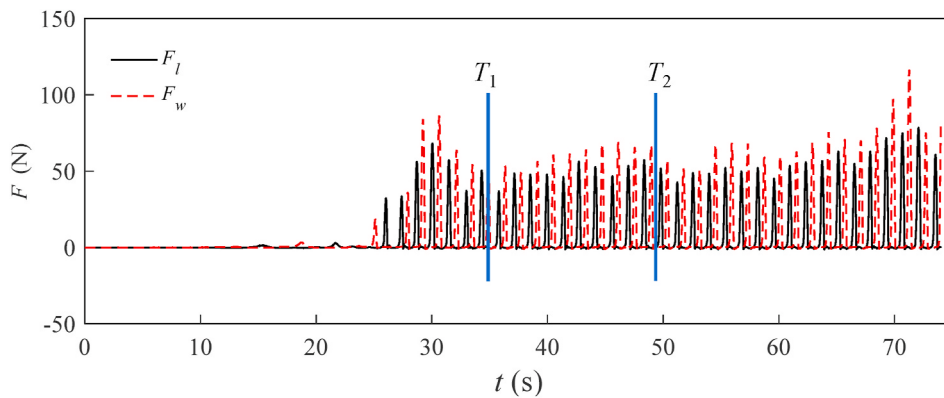


Fig. A2. Time histories of mooring force η_F for Type C floating breakwater at: $H = 0.10$ m and $T = 1.4$ s.

References

- Black, J.L., Mei, C.C., Bray, M.C.G., 1971. Radiation and scattering of water waves by rigid bodies. *J. Fluid Mech.* 46 (1), 151–164.
- Cui, J., Liu, H., Deng, X., Tao, S., Li, Q., 2019. An experimental study on hydrodynamic performance of a box-floating breakwater in different terrains. *J. Mar. Sci. Technol.* 1–19.
- Dai, J., Wang, C.M., Utsunomiya, T., Duan, W., 2018. Review of recent research and developments on floating breakwaters. *Ocean Eng.* 158, 132–151.
- Dean, R., Dalrymple, R.A., 1984. *Wave Mechanics for Engineering and Scientists*. World Scientific Publishing Company.
- Dong, G.H., Zheng, Y.N., Li, Y.C., Teng, B., Guan, C.T., Lin, D.F., 2008. Experiments on wave transmission coefficients of floating breakwaters. *Ocean Eng.* 35 (8–9), 931–938.
- Drimer, A., Agnon, Y., Stiassnie, M., 1992. A simplified analytical model for a floating breakwater in water of finite depth. *Appl. Ocean Res.* 14 (1), 33–41.
- Elchahal, G., Younes, R., Lafon, P., 2009. Parametrical and motion analysis of a moored rectangular floating breakwater. *J. Offshore Mech. Arctic Eng.* 131 (3), 1672–1682.
- Goda, Y., Suzuki, Y., 1976. Estimation of incident and reflected waves in random wave experiments. In: Proceedings of the 15th Coastal Engineering Conference, pp. 828–845.
- He, F., Huang, Z., Law, A.W.-K., 2013. An experimental study of a floating breakwater with asymmetric pneumatic chambers for wave energy extraction. *Appl. Energy* 106, 222–231.
- He, F., Huang, Z., Wing-Keung Law, A., 2012. Hydrodynamic performance of a rectangular floating breakwater with and without pneumatic chambers: an experimental study. *Ocean Eng.* 51, 16–27.
- Huang, Z., He, F., Zhang, W., 2014. A floating box-type breakwater with slotted barriers. *J. Hydraul. Res.* 52 (5), 720–727.
- Islam, H., Mohapatra, S.C., Gadelho, J., Guedes Soares, C., 2019. OpenFOAM analysis of the wave radiation by a box-type floating structure. *Ocean Eng.* 193.
- Jalani, M.A., Ismail, N.I., Saad, M.R., Samion, M.K.H., Imai, Y., Nagata, S., Rahman, M.R. A., 2022. Experimental study on a bottom corner of the floating WEC. *Ocean Eng.* 243, 110237.
- Ji, C., Deng, X., Cheng, Y., 2018. An experimental study of double-row floating breakwaters. *J. Mar. Sci. Technol.* 24 (2), 359–371.
- Koutandos, E., Prinos, P., Gironella, X., 2010. Floating breakwaters under regular and irregular wave forcing: reflection and transmission characteristics. *J. Hydraul. Res.* 43 (2), 174–188.
- Liu, Y., Li, H.-J., Li, Y.-C., 2012. A new analytical solution for wave scattering by a submerged horizontal porous plate with finite thickness. *Ocean Eng.* 42, 83–92.
- Liu, Z., Wang, Y., 2020. Numerical investigations and optimizations of typical submerged box-type floating breakwaters using SPH. *Ocean Eng.* 209.
- Liu, Z., Wang, Y., Wang, W., Hua, X., 2019. Numerical modeling and optimization of a winged box-type floating breakwater by Smoothed Particle Hydrodynamics. *Ocean Eng.* 188.
- Loukogeorgaki, E., Yagci, O., Sedat Kabdasli, M., 2014. 3D Experimental investigation of the structural response and the effectiveness of a moored floating breakwater with flexibly connected modules. *Coast. Eng.* 91, 164–180.
- Masoudi, E., Gan, L., 2020. Diffraction waves on large aspect ratio rectangular submerged breakwaters. *Ocean Eng.* 209.
- Ning, D., Zhao, X., Göteman, M., Kang, H., 2016. Hydrodynamic performance of a pile-restrained WEC-type floating breakwater: an experimental study. *Renew. Energy* 95, 531–541.
- Peña, E., Ferreras, J., Sanchez-Tembleque, F., 2011. Experimental study on wave transmission coefficient, mooring lines and module connector forces with different designs of floating breakwaters. *Ocean Eng.* 38 (10), 1150–1160.
- Peng, W., Lee, K.-H., Shin, S.-H., Mizutani, N., 2013. Numerical simulation of interactions between water waves and inclined-moored submerged floating breakwaters. *Coast. Eng.* 82, 76–87.
- Rahman, M.A., Mizutani, N., Kawasaki, K., 2006. Numerical modeling of dynamic responses and mooring forces of submerged floating breakwater. *Coast. Eng.* 53 (10), 799–815.

- Ren, B., He, M., Li, Y., Dong, P., 2017. Application of smoothed particle hydrodynamics for modeling the wave-moored floating breakwater interaction. *Appl. Ocean Res.* 67, 277–290.
- Ruol, P., Martinelli, L., Pezzutto, P., 2013. Formula to predict transmission for π -type floating breakwaters. *J. Waterw. Port, Coast. Ocean Eng.* 139 (1), 1–8.
- Saghi, H., Mikkola, T., Hirdaris, S., 2021. A machine learning method for the evaluation of hydrodynamic performance of floating breakwaters in waves. *Ships Offshore Struct.* 12, 1–15.
- Sannasiraj, S.A., Sundar, V., Sundaravadiel, R., 1998. Mooring forces and motion responses of pontoon-type floating breakwaters. *Ocean Eng.* 25 (1), 27–48.
- Sutko, A.A., 1975. Floating breakwaters - a wave tank study. *J. Petrol. Technol.* 27 (3), 269–273.
- Wang, C.M., Tay, Z.Y., Takagi, K., Utsunomiya, T., 2010. Literature Review of methods for mitigating hydroelastic response of VLFS under wave action. *Appl. Mech. Rev.* 63 (3), 651–664.
- Yamamoto, T., Yoshida, A., Ijima, T., 1980. Dynamics of elastically moored floating objects. *Appl. Ocean Res.* 2 (2), 85–92.
- Yoon, J.-S., Ha, T., Jung, J., 2018. Laboratory experiments on characteristics of perforated-type floating breakwaters. *J. Coast Res.* 85, 1051–1055.
- Zhao, X., Ning, D., 2018. Experimental investigation of breakwater-type WEC composed of both stationary and floating pontoons. *Energy* 155, 226–233.
- Zhao, X., Ning, D., Liang, D., 2019. Experimental investigation on hydrodynamic performance of a breakwater-integrated WEC system. *Ocean Eng.* 171, 25–32.
- Zheng, S., Zhang, Y., 2015. Wave diffraction and radiation by multiple rectangular floaters. *J. Hydraul. Res.* 54 (1), 102–115.
- Zheng, Y.H., You, Y.G., Shen, Y.M., 2004. On the radiation and diffraction of water waves by a rectangular buoy. *Ocean Eng.* 31 (8–9), 1063–1082.